Article

Tin Assisted Fully Exposed Platinum Clusters Stabilized on Defect-Rich Graphene for Dehydrogenation Reaction

Jiayun Zhang, Yuchen Deng, Xiangbin Cai, Yunlei Chen, Mi Peng, Zhimin Jia, Zheng Jiang, Pengju Ren, Siyu Yao, Jinglin Xie, Dequan Xiao, Xiao-Dong Wen, Ning Wang, Hongyang Liu, and Ding Ma

ACS Catal., **Just Accepted Manuscript** • Publication Date (Web): 27 Mar 2019

Tin Assisted Fully Exposed Platinum Clusters Stabilized on Defect-Rich Graphene for Dehydrogenation Reaction

*Jiayun Zhang,[1, 2 #] Yuchen Deng,[3#] Xiangbin Cai,[4 #] Yunlei Chen,[5, 6 #] Mi Peng,[3] Zhimin Jia, [1, 2] Zheng Jiang,[7] Pengju Ren,[5, 6] Siyu Yao,[3] Jinglin Xie,[3] Dequan Xiao,[8] Xiaodong Wen, [5, 6] Ning Wang, [4 *] Hongyang Liu, [1, 2 *] and Ding Ma, [3*]*

[1] Shenyang National Laboratory for Materials Science, Institute of Metal Research, Chinese Academy of Sciences, Shenyang 110016, P. R. China.

[2] School of Materials Science and Engineering, University of Science and Technology of China, Hefei 230026, P. R. China.

[3] Beijing National Laboratory for Molecular Sciences, College of Chemistry and Molecular Engineering and College of Engineering, and BIC-ESAT, Peking University, Beijing 100871, P. R. China.

[4] Department of Physics and Center for Quantum Materials, Hong Kong University of Science and Technology, Clear Water Bay, Kowloon, Hong Kong SAR, P. R. China.

[5] State Key Laboratory of Coal Conversion, Institute Coal Chemistry, Chinese Academy of Sciences, Taiyuan 030001, P. R. China.

[6] University of Chinese Academy of Science, No. 19A Yuanquan Road, Beijing 100049, P. R. China.

[7] Shanghai Institute of Applied Physics, Chinese Academy of Sciences, Shanghai 201204, P. R. China.

[8] Center for Integrative Materials Discovery, Department of Chemistry and Chemical Engineering, University of New Haven, 300 Boston Post Road, West Haven, Connecticut 06516, United States.

[#] These authors contributed equally to this work.

Corresponding authors: *Hongyang Liu (liuhy@imr.ac.cn), *Ning Wang (phwang@ust.hk) and *Ding Ma (dma@pku.edu.cn)

ABSTRACT: Tin assisted fully exposed Pt clusters are fabricated on the core-shell nanodiamond@graphene (ND@G) hybrid support (a-PtSn/ND@G). The obtained atomically dispersed Pt clusters, with an average Pt atom number of 3, were anchored over the ND@G support by the assistance of Sn atoms as a partition agent and through the Pt-C bond between Pt clusters and defect-rich graphene nanoshell. The atomically dispersed Pt clusters has guaranteed a full metal availability to the reactants, a high thermal stability as well as an optimized adsorption/desorption behavior. It inhibits the side reactions and enhances catalytic performance in direct dehydrogenation of n-butane at a low temperature of 450 °C, leading to >98% selectivity toward olefin products, and the TOF of a-PtSn/ND@G is approximately 3.9 times higher than that of the traditional Pt3Sn alloy catalyst supported on Al_2O_3 (Pt_3Sn/Al_2O_3).

KEYWORDS: Atomic dispersion, Defect-rich graphene, Pt nanocluster, Dehydrogenation, Heterogeneous catalysis

INTRODUCTION

Light olefins, a widely used feedstock, are important building blocks for the synthesis of polymers and other value-added chemicals.[1-3] Direct dehydrogenation (DDH) of light alkane is a typically industrial process for production of olefin which is an endothermic reaction thus requires high temperatures to obtain satisfactory conversion rates and olefin yields. However, DDH could also lead to serious catalyst deactivation by sintering of active sites and coking at high reaction temperatures.[1, 4] To date, Pt_3Sn alloy catalyst (Pt_3Sn/Al_2O_3) is widely recognized as one of the best catalysts for this reaction, but rapid deactivation is still a main problem because the sintering of Pt_3Sn nanoparticles (NPs) is unavoidable during dehydrogenation process. Meanwhile, only the surface Pt atoms in Pt_3Sn NPs can participate in the catalytic reaction which is uneconomical for Pt utilization. Therefore, developing a better dispersed and more stabilized Pt-based catalyst is pivotal for the DDH of alkanes.

Among all the strategies to increase metal dispersion on support, the most extreme cases aim to create isolated sites or atomically dispersed species on the surface.[5-14] In those cases, each metal atom could be utilized for the reaction and the absence of nearest-neighbor atoms may inhibit the carbonaceous deposition in the reaction according to some reports.[15] In general, the support of catalyst plays an important role in Pt-based catalysts.[11, 16-18] Among various supports, nanocarbons, especially those with functional groups, have drawn much attention, as they can provide abundant surface sites to host metal atoms, forming single-site catalysts[7-9, 19-22] and exhibiting distinct catalytic performance in various reactions.[23-25] The nanodiamond (ND) is a unique class of nanocarbon materials. The native ND or those after various treatments

is an ideal platform for the host of metal NPs.[26] We have demonstrated recently that after a thermal treatment, the surface of ND can be reconstructed into an ultrathin, curved and defect-rich sp2 graphene nanoshell reinforced by a sp3 diamond nanocore (ND@G) which could anchor isolated Pd atoms through Pd-C bond to obtain atomically dispersed Pd catalysts.[27]

Herein, we report a method to construct Pt-Sn catalyst with unique Pt species, i.e., fully exposed Pt clusters anchoring over the ND@G support (a-PtSn/ND@G). By the strong interaction with the support and also the partitioning role of homogenously dispersed Sn species, Pt atoms were atomically dispersed over the surface of ND@G. The stable Pt clusters with average Pt atom number of 3 were constructed. The as-synthesized a-PtSn/ND@G catalyst shows excellent catalytic performance in DDH of n-butane at a relatively low temperature (i.e., 450 ^{o}C), benefiting from the efficient use of Pt atoms and easy desorption of butene from these stable fully exposed Pt clusters.

RESULTS and DISCUSSION

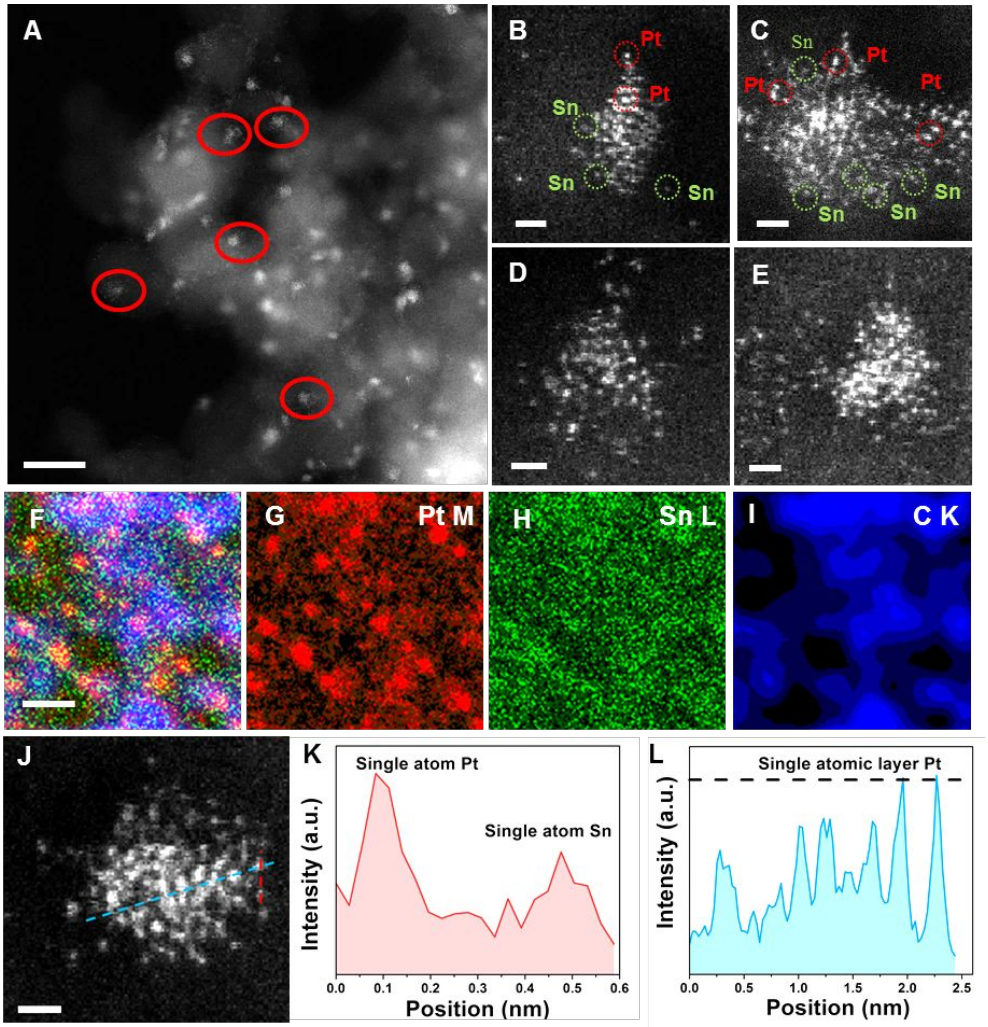

Figure 1. HAADF-STEM images of the a-PtSn/ND@G catalyst, A) Showing the homogeneous distribution of Pt clusters, scale bar, 10 nm, and B-E) the atomic dispersion of Pt and Sn, scale bar, 0.5 nm. Some Pt and Sn atoms in image B and C are marked by red and green circles according to the Z-contrast mechanism, respectively. F-I) Energy-dispersive X-ray (EDX) mapping spectroscopy showing the composition maps of the a-PtSn/ND@G catalyst, scale bar, 10 nm. J) HAADF-STEM image of a-PtSn/ND@G and the extracted line profiles K, L) along red and blue directions in J), demonstrating the pronounced intensity difference between Pt and Sn, consistent well with their distinct atomic numbers (Z), together with the single-atomic-layer thickness of a typical PtSn cluster, scale bar, 0.5 nm.

The a-PtSn/ND@G catalyst was prepared by impregnation of a solution of Pt and Sn precursors over the ND@G hybrid support with a diamond core and a thin graphene shell decorated with abundant defects formed during the annealing of nanodiamond (TEM images see fig. S1A-B). Meanwhile, as the control, a Pt/ND@G with the same Pt loading but without addition of Sn was prepared. It is clear from XRD profiles of both catalysts that the Pt and Sn species did not form large NPs over the surface of ND@G (fig. S2A). The aberration-corrected high-angle annular dark-field scanning transmission electron microscopy (HAADF-STEM) was then employed to study the detailed structure of Pt and Sn on ND@G (Fig. 1). Notably, lots of island-like aggregates (1-2 nm in size, marked in red circles) were observed on ND@G support as shown in Fig. 1A, while no crystalized Pt NPs were observed. The zoomed-in images (Fig. 1B-E) of these island-like aggregates showed that the Pt clusters were randomly distributed on the ND@G surface with irregular shapes (marked in red circles). The mono-dispersed Sn species were also observed on adjacent area (marked in green circles). The co-existence of Pt clusters and mono-dispersed Sn atoms was further confirmed by the EDX mapping (Fig. 1F-I), as distinct distribution forms of Pt (red) and Sn (green) were clearly resolved on the carbon support (blue). These results demonstrated that the irregular island-like Pt aggregates were composed of irregular ultra-small Pt clusters with Pt atom number ranging from 1 to few, partitioned by surrounding mono-dispersed Sn atoms. Significantly, these ultra-small Pt clusters were one-atomic-layer thick (Fig. 1J-L and fig. S4 A-F), indicating a maximum dispersion of all Pt atoms, so we termed it as “fully exposed Pt clusters”. A further H_2/O_2 titration

measurement (Table S1) showed that for the a-PtSn/ND@G catalyst, the dispersion of Pt is 99.2%, further confirming that almost all the Pt atoms were fully exposed on the ND@G surface, consistent well with the HAADF-STEM results.

In order to investigate the dispersion of Sn species on ND@G, HAADF-STEM images of the Sn/ND@G were recorded (fig. S1C-F), where the loading amount of Sn is identical to that of a-PtSn/ND@G, but without adding Pt. Notably, the Sn species are prone to atomically disperse on the defect-rich graphene nanoshell as marked in fig. S1F, which has the same feature as that in a-PtSn/ND@G catalyst. However, for Pt catalyst without adding Sn in the preparation step, the structure of the obtained catalyst, Pt/ND@G, changed significantly. Different from that of a-PtSn/ND@G with only fully exposed clusters, Pt species on Pt/ND@G has a different distribution on the surface of the support. The co-existence of the fully exposed Pt clusters and Pt nanoparticles with 3-dimensional lattice structure were clearly resolved on Pt/ND@G, as marked in fig. S3B. The aggregation of Pt atoms also caused a decrease in Pt dispersion (Table S1). The results indicate that the co-existence of atomically dispersed Sn species has a critical influence over the dispersion of Pt on ND@G support. Without the assistance of the mono-dispersed Sn species, Pt species tend to aggregate to form crystalized NPs and cannot achieve the high dispersion as that of a-PtSn/ND@G catalyst, which inevitably lead to significant difference on the corresponding catalytic performance.

In addition, a typical previous reported PtSn alloy (Pt_3Sn alloy) catalyst (Pt_3Sn/Al_2O_3) with high activity in DDH of alkane reaction was prepared as well.[16] Fig. S3C-K shows typical HAADF-STEM images of Pt_3Sn/Al_2O_3 catalyst. A relatively broad distribution

of metal NPs on Al_2O_3 was observed (fig. S3D). No diffraction peaks related with Pt, Sn or Pt-Sn species were resolved on alumina (fig. S2A), due to the overlapping of the diffraction peaks. EDX mapping analysis (fig. S3H-K) illustrate that Pt and Sn species are uniformly existed in the same nanoparticles. Pt_3Sn alloy was further confirmed by lattice distance of 0.406nm (the lattice distance of $Pt_3Sn(100)$ is 0.4004 nm PDF#65-0958) (fig. S3E-G), providing the further evidence that Sn was alloyed with Pt to form Pt_3Sn alloy nanoparticles on Al_2O_3 support.

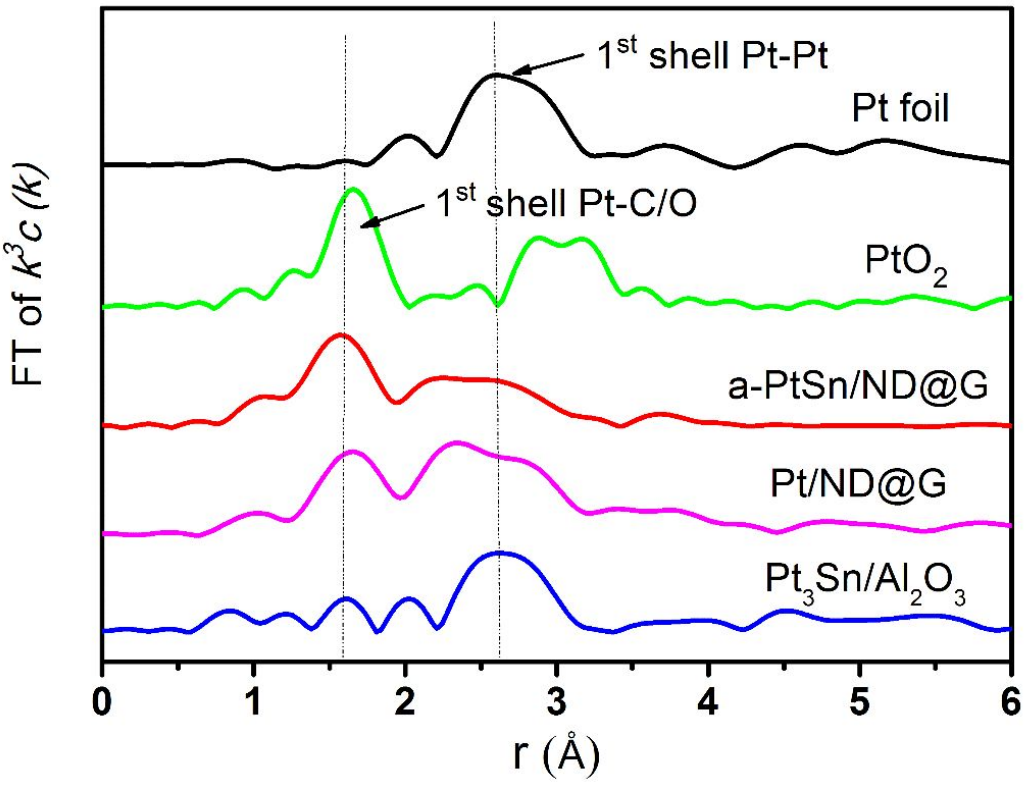

Figure 2. FT-EXAFS profiles of different catalysts**,** a-PtSn/ND@G, Pt/ND@G, Pt_3Sn/Al_2O_3, Pt foil and PtO_2.

The structure and the local environment of Pt and Sn species were further investigated by the extended X-ray absorption fine structure (EXAFS) spectroscopy. The Fourier-transformed (FT) k^3-weighted EXAFS at the Pt L_3-edge is shown in Fig. 2. For the a-PtSn/ND@G catalyst, a distinct peak at 1.6 Å and a relatively weaker peak at 2.6 Å were observed, corresponding to Pt-C/O and Pt-Pt first coordination shells, respectively. For the Pt/ND@G catalyst, the Pt-Pt coordination peak at 2.6 Å were relatively stronger than Pt-C/O coordination peak. The relative intensity of two peaks in a-PtSn/ND@G and Pt/ND@G is more clearly presented in wavelet transformation (WT) of Pt L_3-edge EXAFS oscillations in Fig. 3A-B. For Pt/ND@G (Fig 3B), the relatively stronger signal at 2.6 Å (corresponds to Pt-Pt coordination, fig. S5) than the signal at 1.6 Å (corresponds to Pt-O/C coordination, fig. S5) implying the existence of Pt NPs with larger average Pt-Pt coordination number (C.N.), which agrees well with the results of HAADF-STEM and H_2/O_2 titration measurement. The structure of Sn species was also confirmed by XAFS characterization. As shown in XANES spectra of Sn K-edge (fig S6), the adsorption edge of Sn in a-PtSn/ND@G is close to SnO_2, indicating that the high dispersion of Sn lead to an increased average chemical valance. The Fourier-transformed (FT) k^2-weighted EXAFS at the Sn K-edge (fig S7) also showed that no Sn-O-Sn coordination signal was observed, which again confirmed the atomic dispersion of Sn. As for Pt_3Sn/Al_2O_3, the only peak at around 2.6 Å belongs to the first coordination shell of Pt-Pt/Sn (Fig.2). The strong intensity of the peak implies the formation of PtSn alloy nanoparticles which agrees well with HAADF-STEM results

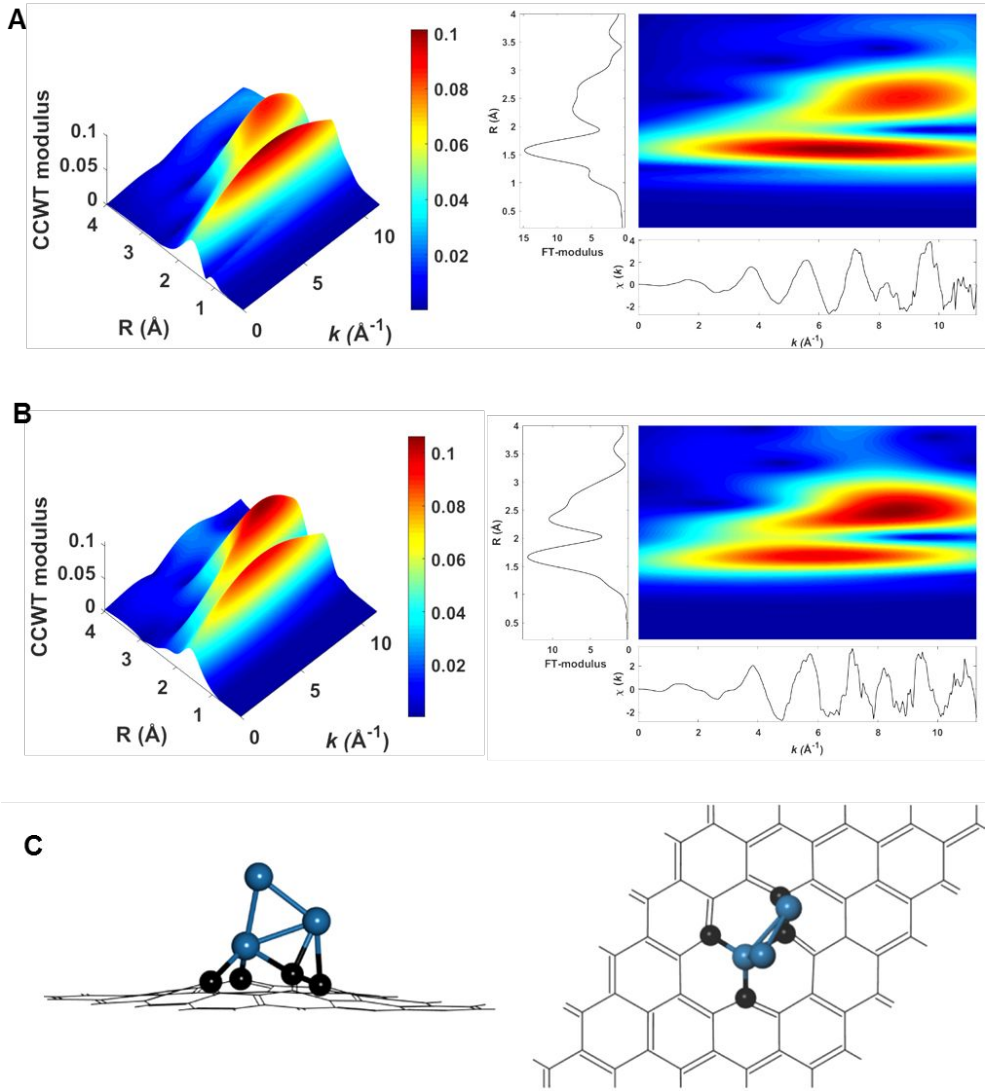

Figure 3. Wavelet transform (WT) analysis of different catalysts, A) a-PtSn/ND@G and B) Pt/ND@G. C) The optimized structure of Pt_3 cluster embedded into graphene (Pt_3-Gr, through Pt-C bond) from top and side view.

The detailed EXAFS fitting parameters of these catalysts are shown in Table S2 and fig. S8-9. For a-PtSn/ND@G, the average C.N. of Pt-C/O is 2.2, and the average C.N. of Pt-Pt is only 1.8. In comparison, the average C.N. of Pt-Pt in Pt/ND@G is 4.8. The result confirmed the presence of ultra-small Pt clusters in the a-PtSn/ND@G catalyst (Pt-Pt coordination number around 2 (1.8)), revealing that each ultra-small Pt clusters

has an average Pt atom number of 3. This means all the Pt atoms in the catalyst are available for adsorptions and reactions. To further investigate the local coordination structure of Pt species, DFT calculations were used to investigate different bonding models of atomically dispersed Pt_3-(C/O)x clusters on ND@G. We use a cluster with 3 Pt atoms to represent the atomically dispersed Pt cluster species. The optimized geometry of the Pt_3 cluster is shown in Fig. 3C. It was clear that a Pt_3 cluster was bound to the graphene layer through Pt-C bonds (termed as Pt_3-Gr). Clearly, the optimized structure of the triangular Pt_3 cluster was not in parallel with carbon support surface, which may explain the irregular atomic structures of Pt clusters under STEM due to the projection nature of TEM imaging (fig. S4G-J). The average Pt-C bond length was 2.05 Å, in consistent with the experimental observation of the Pt-C bond length (2.02±0.02 Å) in the first coordination shell (Table S2), suggesting the validity of current model.

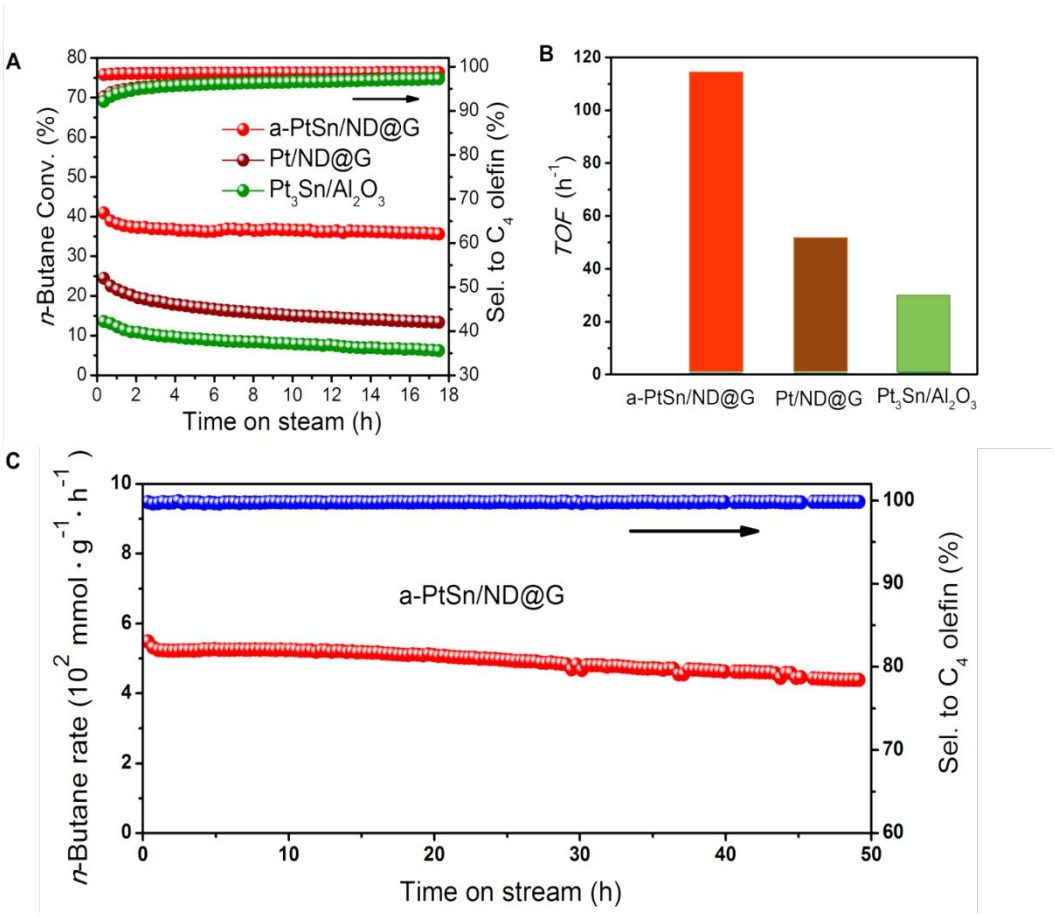

Figure 4. Direct dehydrogenation of n-butane over the different catalysts, A) Conversion and selectivity by time-on-stream during DDH of n-butane at 450 °C. GHSV=18000 $mL \cdot g_{cat}^{-1} \cdot h^{-1}$, $nC_4:H_2=1:1$ with He balance. B) The turnover frequency (TOF) for a-PtSn/ND@G, Pt_3Sn/Al_2O_3 and Pt/ND@G. C) Stability test at 450 °C.

We then evaluated the direct dehydrogenation of n-butane over the a-PtSn/ND@G catalyst under atmospheric pressure at 450 °C, with Pt/ND@G, Sn/ND@G and Pt_3Sn/Al_2O_3 as references. As shown in Fig. 4A and Table S3, the initial conversion of the Pt_3Sn/Al_2O_3 catalyst was 13.6%, and the selectivity to total C_4 olefin (e.g., n-butene, 1, 3-butadiene) was 92.1%. However, the activity experienced a sharp decline to 9.5% in 4 h and gradually decreased to 6.2% in 18 h. As to Pt/ND@G, although the initial

conversion (24.4%) is higher than that of Pt_3Sn/Al_2O_3 catalyst (13.6%), a quick deactivation also happened causing conversion dropped from 24.4% to 13.4% in 18 h test, which is agree with the reaction behavior of Pt_3Sn catalyst previously reported. Deactivation was observed for both Pt/ND@G and Pt_3Sn/Al_2O_3 catalysts, which may result from coke deposition and/or sintering of active centers. In addition, the Sn/ND@G catalyst did not show any activity under the reaction condition, providing the further evidence that mono-dispersed Sn species merely work as a partition agent to promote the formation of fully exposed Pt clusters on ND@G. Instead, for the a-PtSn/ND@G catalyst, the initial conversion of n-butane was as high as 40.9%, and the selectivity of C_4 olefin reached 98.2%. Significantly, only a slight deactivation after 18 h (from 40.9% to 35.6%) was observed. In a long-term reaction test, the activity of a-PtSn/ND@G (Fig. 4C) remained at a rather high level, and the selectivity toward C_4 olefin was >98% after 50 h reaction. Atomic images of the used catalyst (fig. S10) showed the structures of atomically dispersed Pt clusters were well preserved after the reaction (in 18 h), and the dispersion of Pt in the used a-PtSn/ND@G catalyst was 97.3% (Table S1), indicated that nearly all the Pt atoms remained atomically exposed. Moreover, the Pt-based activity of a-PtSn/ND@G reached 114 h^{-1}, which was approximately 3.9 times as that of Pt_3Sn/Al_2O_3 and 2.2 times as that of Pt/ND@G catalyst, respectively (Fig. 4B). These results demonstrated that the atomic dispersion of Pt clusters could promise a maximum utilization of Pt atoms during the DDH reaction of butane, while the improved longevity of a-PtSn/ND@G might be ascribed to the stabilization effect conferred by partition agents, Sn species.

Another possible reason for the high activity and stability of a-PtSn/ND@G may originate from the distinct adsorption/desorption behavior of reaction species on the catalytic surfaces. From the temperature programmed desorption of n-butene (n-C_4H_8-TPD, fig. S11), it was clear that the adsorption of n-C_4H_8 on atomically dispersed Pt clusters was much weaker than that on the Pt_3Sn alloy. An easier desorption of butene benefited the high reactivity and prevented the aimed product from further deep dehydrogenation to undesired products or coke deposition. From all the results above, we concluded that a-PtSn/ND@G could deliver robust activity, good selectivity, and high stability for the DDH of n-butane, and it was superior to the previously reported Pt-based catalysts as displayed in Table S4.

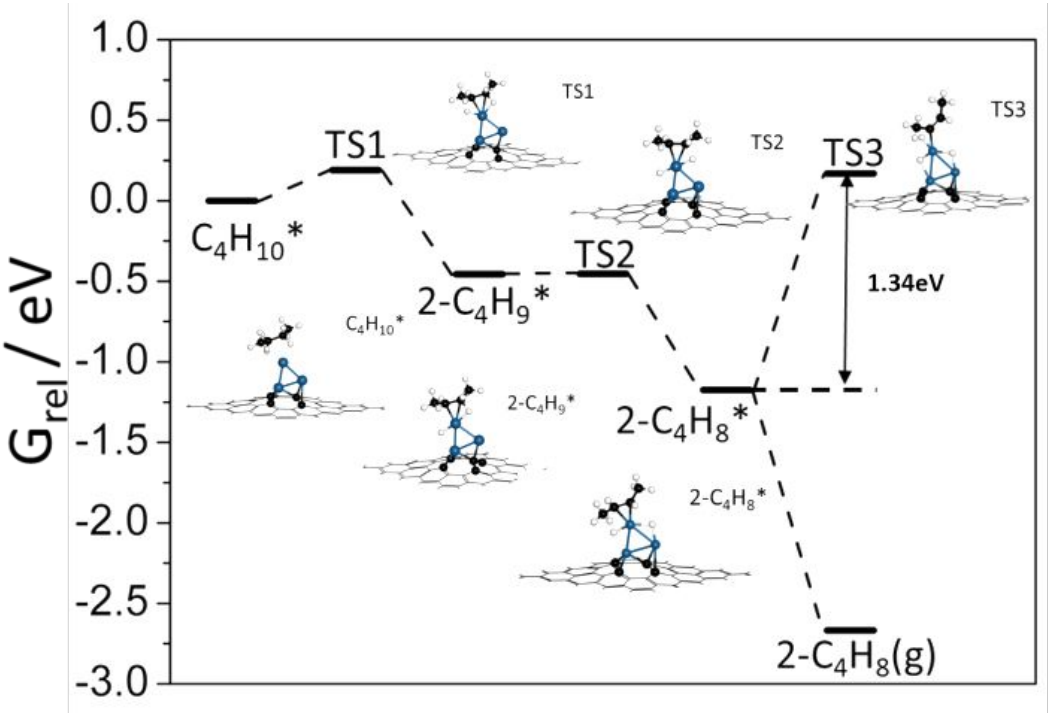

Figure 5. Gibbs free energy profile of direct butane dehydrogenation on the Pt_3-Gr,The structures for intermediates and transition states from C_4H_{10} to 2-C_4H_8 (T = 450 °C).

The reaction mechanism of the DDH reaction over the a-PtSn/ND@G was further studied by the quantum chemistry simulation at the DFT level. Based on structural parameters extracted from quantitative EXAFS curve-fitting, we found that the C.N. of Pt-C/O in the Pt cluster is 2.2, the average Pt-C/O bond length is 2.02 Å, and the C.N. of Pt-Pt is 1.8. Experimental observation suggests that atomically dispersed Pt_3 cluster probably binding with Ox (x=0, 1, 2, 3) species are anchored on graphene due to the indistinguishability of Pt-C or Pt-O bonds in the EXAFS data. Tables S5-7 summarized the potential Pt_3O_x structure and relative stabilities of Pt_3O_x species of different coordination environment. We calculated the change of Gibbs free energies from the most stable Pt_3O_x-graphene to Pt_3-graphene under reaction condition (T = 450 °C, P (H_2) = 0.02 Bar.). Notably, Pt_3O_3-graphene, Pt_3O_2-graphene and Pt_3O_1-graphene will be reduced to Pt_3-graphene under the reaction condition (H_2/Ar=1/9 at 450 °C). Therefore, Pt_3-Gr model is chosen to present the working catalyst to investigate reaction activities and product selectivity.

According to the experimental results, 2-butene was the main product in the DDH reaction. Thus, we focused on the dehydrogenation path from n-butane to 2-butene for the DFT calculations (The Gibbs free energy was calculated based on the temperature of 450 °C). We used Pt_3Sn-(111) as a reference (fig. S12-13) for similar calculations. The calculation result for Pt_3-Gr is shown in Fig. 5, clearly, the dehydrogenation of n-butane to 2-butene followed two steps. Firstly, the initial activation of n-butane occurred at the methylene group on the Pt_3 cluster, leading to the 2-butyl species (2-C_4H_9). Then 2-butene (2-C_4H_8) was formed via further dehydrogenation at methylene

groups of the 2-butyl group. [28] As shown in Table S8, the key energy barrier for the formation of 2-butene was just 0.11 eV on Pt_3-Gr, but 0.72 eV for the (111) surface of Pt_3Sn. The barrier for the deep dehydrogenation of 2-butene was 1.34 eV, higher 0.12 eV than desorption barrier (as shown in Table S10). More importantly, the Gibbs free energy change of 2-butene desorption (ΔG_{des} = -1.54 eV) over Pt3-Gr is highly favorable thermodynamically at 450 ° C, demonstrating the coke deposition was unfavorable on Pt_3-Gr. These results indicated that Pt_3-Gr was more active than Pt_3Sn-(111) for the dehydrogenation of n-butane and apt for the product desorption and thus guarantees a highly selective and coke-resistant catalyst at low reaction temperature. The theoretical results agree well with our experimental observation.

CONCLUSIONS

In summary, we synthesized fully exposed Pt clusters catalyst on ND@G support with the partitioning role of Sn species. The catalyst exhibited excellent catalytic performance for the DDH reaction of n-butane at a temperature as low as 450 ^{o}C. The unique structure of the catalyst guaranteed a fully Pt exposure to the reactants and optimal adsorption/desorption behaviour. These characteristics are pivotal for the design of active, stable and coking-resistant alkane DDH catalysts. The strategy provides a new way to prepare fully exposed metal catalysts and can be extended to other metal catalysts upon further development.

EXPERIMENTAL SECTION

Materials

Nanodiamond (ND) powders were purchased from Beijing Grish Hitech Co., China. The γ-Al_2O_3 was also purchased from Aladdin. Analytical grade chloroplatinic acid ($H_2PtCl_6·6H_2O$) and Tin (II) chloride dehydrate ($SnCl_2·2H_2O$) were purchased from Sinopharm Co. Ltd.

Catalysts preparation

The nanodiamond@graphene (ND@G) hybrid carbon support was synthesized by thermal annealing of fresh ND powder at 1100 ^oC under Ar flow (80 mL•min^{-1}) for 4 h. The a-PtSn/ND@G catalyst was prepared by co-impregnation method using $H_2PtCl_6·6H_2O$ and $SnCl_2·2H_2O$ as the precursors. Typically, certain amount of H_2PtCl_6 (equivalent to 1.0 wt% Pt weight loading on ND@G support) and $SnCl_2·2H_2O$ (Sn/Pt atomic ratio: 1.7/1) were dissolved in 2 ml ethanol. The solution was impregnated into the ND@G powder (200 mg), under stirring at room temperature for 20 h. Then, the samples were dried at 40 ^oC for another 6 h. Finally, the samples were calcined in Ar (80 mL•min^{-1}) at 500 ^oC for 4 h and then reduced in H_2 gas (80 mL•min-1) at 500 ^oC for another 1h. For reference, the Pt/ND@G with 1.0 wt% Pt weight loading was prepared with the similar process without the addition of Sn and the Sn/ND@G with 0.5 wt% was prepared with the similar process without the addition of Pt. A γ-Al_2O_3 supported Pt_3Sn alloy catalyst (1.0 wt% Pt, Sn/Pt atomic ratio: 0.5/1) was also prepared using the same preparation procedure as mentioned above and named as Pt_3Sn/Al_2O_3.

Characterizations

The crystal structure of the samples were characterized by X-ray diffraction (XRD) on a D/MAX-2500 PC X-ray diffractometer with monochromated Cu K radiation (λ=1.54

Å). Atomic micrographs were collected on a JEOL JEM ARM 200CF aberration-corrected scanning transmission electron microscope at 200 kV accelerating voltage. XPS was carried out on ESCALAB 250 with monochromated Al Kα radiation, at a pass energy of 50 eV; the spectra were calibrated using the adventitious carbon C–C peak to 284.8 eV. The extend X-ray absorption spectra were collected at beamline (BL14W1) at the Shanghai Synchrotron Radiation Facility. The BET surface area, BJH pore volume and the average pore diameter of the as-prepared samples were measured by N2 adsorption isotherm on a Micromeritics ASAP 2020 analyzer. Temperature-programmed desorption of n-butene (n-C_4H_8) was conducted in He atmosphere. Typically, the samples (50 mg) were first treated in flowing He (30 mL•min^{-1}) at 30 ^{o}C for 1 h. Then, He was switch to a flowing C_4H_8 (15 mL•min^{-1}) and treated at the same temperature for 30 min. After that, the system was swept in a flowing He stream (30min mL•min^{-1}) until a stable baseline was obtained. The temperature of the catalyst was then increased from 30 ^{o}C to 450 ^{o}C (ramping rate: 5 ^{o}C /min) in flowing He (30 mL•min^{-1}) and the MS signals (mass spectrometer: Pfeiffer-omnistar) of the reactant/product were recorded. The H_2-O_2 titration measurements were performed on a Micromeritics AutoChem II 2920 equipped with a thermal conductive detector.

Reaction evaluation

The catalytic performance for the DDH reaction of n-butane was tested in a fixed-bed stainless steel micro-reactor with a quartz lining under atmosphere pressure at 450 ^{o}C using 50 mg catalyst plugged in with quartz wool at the center of the quartz lining. The reaction was carried out in a feed gas with a composition of 2% H_2, 2% n-C_4H_{10} and

He as carrier gas, and a gas hour space velocity (GHSV) of 18000 $mL \cdot g_{cat}^{-1} \cdot h^{-1}$ on the basis of the whole feed gas (the total flow rate is 15 $mL \cdot min^{-1}$). The effluent mixture gas was analyzed by on-line gas chromatography (Agilent 7890 with a FID and a TCD detector). The rate and conversion of n-butane and the selectivity of total C_4 olefin (n-butene and 1, 3-butadiene) were calculated using the following equations:

n-Butane Conversion: conv. = (mol of the reacted) / (mol of inlet n-butane) x 100%

(1)

Selectivity of C_4 olefin: Selectivity = {mol of (butene formed + 1, 3-butadiene formed)} / (mol of reacted) × 100%

(2)

n-butane rate = (flow rate of n-butane × conversion of n-butane × 60)/(weight of Pt in the catalyst × 22.4)

(3)

The catalyst stability was described by a first-order deactivation model:

$k_d = \{\ln[(1-C_f) / C_f] - \ln[(1-C_i) / C_i]\}/t$

(4)

C_i: initial conversion after reaction 30 min. C_f: final conversion value. Where t represents the reaction time (h), and k_d is the deactivation rate constant (h^{-1}) which is used to evaluate the catalyst stability (higher k_d values, lower stability).

Computational details

All calculations were performed using the plane-wave based DFT method implemented in the Vienna Ab Initio Simulation Package (VASP).[29-30] We describe the electron–ion

interaction using the projector augmented wave (PAW) method.[31-32] The generalized gradient approximation and the Perdew–Burke–Ernzerhof functional (GGA-PBE)[33] describes the exchange and correlation energies for all systems. The plane wave expansion of the wave functions adopted an energy cut-off of 400 eV. The ground-state structure of bulk and surfaces were obtained by minimizing forces with the conjugate-gradient algorithm until the force on each ion is below 0.02 eV/Å and the convergence criteria for electronic self-consistent interactions is 10^{-5}.

Perfect and defective graphene have been widely use as support of noble metal theoretical studies[34-36]. Here, Pt_3 cluster embedded into a monovacancy at 5×5 super cell of graphene was adopted as model to simulate the active site of butane dehydrogenation (Pt_3-Gr) through comparative investigation between potential Pt cluster models and EXAFS data. The vacuum layer was set to 20 Å to avoid interaction from adjacent cells. The Monkhorst-Pack k-point set to 3×3×1 in the reciprocal lattice, and the electronic occupancies were determined according to the Gaussian smearing method with σ = 0.1 eV. Spin−polarized calculations have been performed. For Pt_3Sn (111) surface, a four-layer slab with a ($2\sqrt{3} \times 2\sqrt{3}$) R30° supercell (Totally 48 atoms) was used to represent the Pt3Sn alloyed surfaces, achieving the coverage of adsorbates of 1/12 ML. The successive slabs were separated by a vacuum region as thick as 20 Å to eliminate periodic interactions. The Brillouin zone is sampled with a 2×2×1 k-points mesh by the Monkhorst–Pack algorithm. The electronic occupancies were determined according to the Methfessel-Paxton scheme with σ = 0.2 eV. The bottom one layers of

the slab were kept fixed to their crystal lattice positions. Spin-polarization is not considered in Pt_3Sn (111) calculation.

The most stable configurations of the reactants and intermediates on Pt_3-Gr and Pt_3Sn (111) surface were obtained by the standard minimization of density functional theory (DFT). These configurations were used as the initial state, from which the constrained optimization method as described by Plessow[36] was used to search the transition states (TS). The TS optimization convergence was regarded to be achieved when the force on each atom was less than 0.05 eV/Å. All transition states have been verified to include only one imaginary harmonic frequency corresponding to the transition vector of the reaction. Furthermore, small distortions along the transition vector followed by optimization toward the minima verified the connectivity of the transition states.

We have considered zero-point energies (ZPE) of reaction species and transition states during the dehydrogenation of n-butane. Gibbs free energies for the gas-phase species were determined by combining electronic and ZPE with entropy (T=450 °C). For chemisorbed reaction species, only the electronic energy and ZPE was included in the calculation of the Gibbs free energy.

Potential Models of Pt_3O_x-graphene according to EXAFS data. Based on structural parameters extracted from quantitative EXAFS curve-fitting, we found that the C.N. of Pt-C/O in the Pt cluster is 2.2, the average Pt-C/O bond length is 2.02 Å, and the C.N. of Pt-Pt is 1.8. Experimental observation suggests that atomically dispersed Pt_3 cluster binding with O_x (x=0, 1, 2, 3) species are anchored on graphene due to the indistinguishability of Pt-C or Pt-O bonds in the EXAFS data. Table S6-8 summarized

the potential Pt_3O_x structure and relative stabilities of Pt_3O_x species of different coordination environments.

ASSOCIATED CONTENT

Supporting Information

The Supporting Information is available free of charge on the ACS Publications website. Supplementary characterization and activation calculation results (Figures S1-S13, Tables S1-S10) as described in the text.

AUTHOR INFORMATION

Corresponding Authors

*Hongyang Liu (liuhy@imr.ac.cn), *Ning Wang (phwang@ust.hk) and *Ding Ma (dma@pku.edu.cn)

ORCID

Hongyang Liu: 0000-0003-2977-2867

Ning Wang: 0000-0002-4902-5589

Ding Ma: 0000-0002-3341-2998

Notes

The authors declare no competing financial interest.

ACKNOWLEDGMENTS

This work was supported by the MOST (2016YFA0204100, 2017YFB0602200), the NSFC of China ((91845201, 21573254, 91545110, 21725301, 91645115, 21473003 and 21821004), the Youth Innovation Promotion Association, Chinese Academy of Science (CAS). N. W. acknowledges the funding support from the Research Grants Council of Hong Kong (Project Nos. C6021-14E and 16306818).

REFERENCES

(1) Sattler, J.; Ruiz-Martinez, J.; Santillan-Jimenez, E.; and Weckhuysen, B. M. Catalytic dehydrogenation of light alkanes on metals and metal oxides. *Chem. Rev.* **2017**, 114, 10613-10653.

(2) McFarland, E. Unconventional chemistry for unconventional natural gas. *Science* **2012**, **338**, 340-342.

(3) Weckhuysen, B. M. and Schoonheydt, R. Alkane dehydrogenation over supported chromium oxide catalysts. *Catal. Today*. **1999**, 51, 223-232.

(4) Xu, Y.; Lu, J.; Zhong, M. and Wang, J. J. Dehydrogenation of n-butane over vanadia catalysts supported on silica gel. *J. Nat. Gas Chem.* **2009***,* 18, 88-93.

(5) Qiao, B. T.; Wang, A.; Yang, X.; Allard, L. F.; Jiang, Z.; Cui, Y.; Liu, J.; Li, J.; Zhang, T. Single-atom catalysis of CO oxidation using Pt_1/FeO_x. *Nat. Chem.* **2011**, 3, 634-641.

(6) Lin, L.; Zhou, W.; Gao, R.; Yao, S.; Zhang, X.; Xu, W.; Zheng, S.; Jiang, Z.; Yu, Q.; Li, Y. W.; Shi, C.; Wen, X. D.; Ma, D. Low-temperature hydrogen production from water and methanol using Pt/α-MoC catalysts. *Nature* **2017**, 544, 80-83.

(7) Chen, Z.; Vorobyeva, E.; Mitchell, S.; Fako, E.; Ortuño, M. A.; López, N.; Collins, S. M.; Midgley, P. A.; Richard, S.; Vilé, G.; Pérez-Ramírez, J. A heterogeneous single-atom palladium catalyst surpassing homogeneous systems for suzuki coupling. *Nat. Nanotechnol.* **2018**, 13, 702–707.

(8) Chen, Z.; Mitchell, S.; Vorobyeva, E.; Leary R. K.; Hauert R.; Furnival T.; Ramasse Q. M.; Thomas J. M.; Midgley P. A.; Dontsova D.; Antonietti M.; Pogodin S.; Pérez-Ramírez, J. Stabilization of single metal atoms on graphitic carbon nitride. *Adv. Funct. Mater.* **2017***,* 27, 1605785.

(9) Mitchell, S.; Vorobyeva, E.; Perez-Ramirez, J. The multifaceted reactivity of single-atom heterogeneous catalysts. *Angew. Chem. Int. Ed.* **2018**, 57, 15316-15329.

(10) Jones, J.; Xiong, H.; DeLaRiva, A. T.; Peterson, E. J.; Pham, H.; Challa, S. R.; Qi, G.; Oh, S.; Wiebenga, M. H.; Hernández, X. I. P.; Wang, Y.; Datye, A. K. Thermally stable single-atom platinum-on-ceria catalysts via atom trapping. *Science* **2016***,* 353, 150-154.

(11) Nie, L.; Mei, D.; Xiong, H.; Peng, B.; Ren, Z.; Hernandez, X. I. P.; DeLariva, A.; Wang, M.; Engelhard, M. H.; Kovarik, L.; Datye, A. K.; Wang, Y. Activation of surface lattice oxygen in single-atom Pt/CeO_2 for low-temperature CO oxidation. *Science* **2017**, 358, 1419-1423.

(12) Liu, J. C.; Ma, X. L.; Li, Y.; Wang, Y. G.; Xiao, H.; Li, J. Heterogeneous Fe_3 single-cluster catalyst for ammonia synthesis via an associative mechanism. *Nat. Commun.* **2018***,* 9, 1610.

(13) Liu, P.; Zhao Y.; Qin R. X.; Mo S. G.; Chen G. G.; Gu L., Chevrier D. M., Zhang P., Guo Q., Zang D. D.; Wu B. H.; Fu G.; Zheng, N. F. Photochemical route for synthesizing atomically dispersed palladium catalysts. *Science* **2016**, 352, 797-800.

(14) Vignola, E.; Steinmann, S. N.; Mapihan, K. L.; Vandegehuchte, B. D.; Curulla, D.; and Sautet, P. Acetylene adsorption on Pd−Ag alloys: evidence for limited island formation and strong reverse segregation from monte carlo simulations. *J. Phy. Chem. C.* **2018**, 122, 15456-15463.

(15) Guo, X.; Fang, G.; Li, G.; Ma, H.; Fan, H.; Yu, L.; Ma, C.; Wu, X.; Deng, D.; Wei, M.; Li, J.; Sun, L; Tang, Z.; Pan, X.; Bao, X. Direct, nonoxidative conversion of methane to ethylene, aromatics, and hydrogen. *Science* **2014***,* 344, 616-619.

(16) Shi, L.; Deng, G. M.; Li, W. C.; Miao, S.; Wang, Q. N.; Zhang, W. P.; Lu, A. H. Al_2O_3 nanosheets rich in pentacoordinate Al^{3+} ions stabilize Pt-Sn clusters for propane dehydrogenation. *Angew. Chem. Int. Ed.* **2015**, 54, 13994-13998.

(17). Zhu, Y.; An, Z.; Song, H.; Xiang, X.; Yan, W.; He, J. Lattice-confined Sn (IV/II) stabilizing raft-Like Pt clusters: high selectivity and durability in propane dehydrogenation. *ACS Catal.* **2017**, 7, 6973-6978.

(18) Yao, S.; Zhang, X.; Liu; Zhou, W.; Gao R.; Xu, W.; Ye, Y.; Lin L.; Wen, X.; Liu, P.; Chen, B.; Crumlin, E.; Guo, J.; Zuo, Z.; Li, W.; Xie, J.; Lu, L.; Kiely, C. J.; Gu, L.; Shi, C.; Rodriguez, J. A.; Ma, D. Atomic-layered Au clusters on α-MoC as catalysts for the low-temperature water-gas shift reaction. *Science* **2017**, 357, 389-393.

(19) Lit, J. V. D.; Boneschanscher, M. P.; Vanmaekelbergh, D.; I jäs, M.; Uppstu, A.; Ervasti, M.; Harju, A.; Liljeroth, P.; Swart, I. Suppression of electron-vibron coupling in graphene nanoribbons contacted via a single atom. *Nat. Commun.* **2013,** 4, 2023.

(20) Ramasse, Q. M.; Seabourne, C. R.; Kepaptsoglou, D. M.; Zan, R.; Bangert, U.; and Scott, A. J; Probing the Bonding and Electronic Structure of Single Atom Dopants in Graphene with Electron Energy Loss Spectroscopy. *Nano Lett.* **2013,** 13, 498-4995.

(21) Wei, S.; Li, A.; Liu, J. C.; Li, Z.; Chen, W.; Gong, Y.; Zhang, Q.; Cheong, W. C.; Wang, Y.; Zheng, L.; Xiao, H.; Chen, C.; Wang, D.; Peng, Q.; Gu, L.; Han, X.; Li, J.; Li, Y. Direct observation of noble metal nanoparticles transforming to thermally stable single atoms. *Nat. Nanotechnol.* **2018**, 13, 856-861.

(22) Yan, H.; Lin, Y.; Wu, H.; Zhang, W.; Sun, Z.; Cheng, H.; Liu, W.; Wang, C.; Li, J.; Huang, X.; Yao, T.; Yang, J.; Wei, S.; Lu, J. Bottom-up precise synthesis of stable platinum dimers on grapheme. *Nat. Commun.* **2017**, 8, 1070.

(23) Lang, R.; Xi W.; Liu, J.; Cui, T.; Li, T; Lee,A.; Chen, F.; Chen, Y.; Li, L.; Li, L.; Lin, J.; Miao, S.; Liu, X.; Wang, Wang, X.; Luo, J.; Qiao, B. T.; Li, J.; Zhang T. Non defect-stabilized thermally stable single-atom catalyst. *Nat. Commun.* **2019**, 10, 234.

(24) Yan, H.; Cheng, H.; Yi, H.; Lin, Y.; Yao, T.; Wang, C.; Li, J.; Wei, S.; Lu, J Single-atom Pd_1/graphene catalyst achieved by atomic layer deposition: remarkable performance in selective hydrogenation of 1,3-butadiene. *J. Am. Chem. Soc.* **2015***,* 137, 10484-10487.

(25) Vilé, G.; Albani, D.; Nachtegaal, M.; Chen, Z.; Dontsova, D.; Antonietti, M.; López, N.; Pérez-Ramírez, J. A stable single-site palladium catalyst for hydrogenations. *Angew. Chem. Int. Ed.* **2015***,* 54, 11265-11269.

(26) Liu, J.; Yue, Y.; Liu, H.; Da, Z.; Liu, C.; Ma, A.; Rong, J.; Su, D.; Bao, X.; Zheng,H. Origin of the Robust Catalytic Performance of Nanodiamond Graphene Supported Pt Nanoparticles Used in the Propane Dehydrogenation Reaction. *ACS Catal.* **2017**, 7, 3349-3355.

(27) Huang, F.; Deng, Y.; Chen, Y.; Cai, X.; Peng, M.; Xiao, D.; Wen, X.; Wang, N.; Liu, H.; Ma, D. Atomically dispersed Pd on nanodiamond/graphene hybrid for selective hydrogenation of acetylene. *J. Am. Chem. Soc.* **2018**, 140, 13142–13146.

(28) Delbecq, F.; Sautet, P., The effect of substituents on the adsorption of alkenes on (111) Pt and Pd surfaces: a theoretical study. *Catal. Lett.* **1994**, 28, 89-98.

(29) Kresse, G.; Furthmuller, J. Efficient iterative schemes for ab initio total-energy calculations using a plane-wave basis set. *Phys. Rev. B.* **1996**, 54, 11169-11186.

(30) Kresse, G.; Furthmuller, J. Efficiency of ab-initio total energy calculations for metals and semiconductors using a plane-wave basis set. *Comput. Mater. Sci.* **1996**, 6, 15-50.

(31) Blochl, P. E. Projector Augmented-Wave Method. *Phys. Rev. B.* **1994**, 50, 17953-17979.

(32) Kresse, G.; Joubert, D. From ultrasoft pseudopotentials to the projector augmented-wave method. *Phys. Rev. B.* **1999**, 59, 1758-1775.

(33) Perdew, J. P.; Burke, K.; Ernzerhof, M. Generalized gradient approximation made simple *Phys. Rev. Lett.* **1997**, 78, 1396-1396.

(34) Błoński, P.; Hafner, J., Geometric and magnetic properties of Pt clusters supported on graphene: Relativistic density-functional calculations. J. Chem. Phys. 2011, 134, 154705.

(35) Błoński, P.; Dennler, S.; Hafner, J. Strong spin–orbit effects in small Pt clusters: Geometric structure, magnetic isomers and anisotropy. J. Chem. Phys. 2011, 134, 034107.

(36) Plessow, P. N. Efficient Transition State Optimization of Periodic Structures through Automated Relaxed Potential Energy Surface Scans. *J. Chem. Theory. Comput.* **2018**, 14, 981-990.

Table of Contents